JACS Au
AN OPEN ACCESS JOURNAL OF THE AMERICAN CHEMICAL SOCIETY

pubs.acs.org/jacsau
Article

A Reconfigurable DNA Framework Nanotube-Assisted Antiangiogenic Therapy

Wei Li,◆ Zhongliang Wang,◆ Qing Su, Jie Chen, Qian Wu, Xue Sun, Shuhan Zhu, Xiaodie Li, Hao Wei, Jialin Zeng, Linlang Guo,* Chao Zhang,* and Jian He*

Cite This: JACS Au 2024, 4, 1345−1355

Read Online

ACCESS | Metrics & More | Article Recommendations | Supporting Information

ABSTRACT: A major limitation of tumor antiangiogenic therapy is the pronounced off-target effect, which can lead to unavoidable injury in multiple organs. Ensuring sufficient delivery and controlled release of these antiangiogenic agents at tumor sites is crucial for realizing their clinical application. Here, we develop a smart DNA-based nanodrug, termed Endo-rDFN, by precisely assembling the antiangiogenic agent, endostar (Endo), into a reconfigurable DNA framework nanotube (rDFN) that could recognize tumor-overexpressed nucleolin to achieve the targeted delivery and controllable release of Endo. Endo-rDFN can not only effectively enhance the tumor-targeting capability of Endo and maintain its efficient accumulation in tumor tissues but also achieve on-demand release of Endo at tumor sites via the specific DNA aptamer for tumor-overexpressed nucleolin, named AS1411. We also found that Endo-rDFN exhibited significant inhibition of angiogenesis and tumor growth, while also providing effective protection against multiorgan injury (heart, liver, spleen, kidney, lung, etc.) to some extent, without compromising the function of these organs. Our study demonstrates that rDFN represents a promising vector for reducing antiangiogenic therapy-induced multiorgan injury, highlighting its potential for promoting the clinical application of antiangiogenic agents.

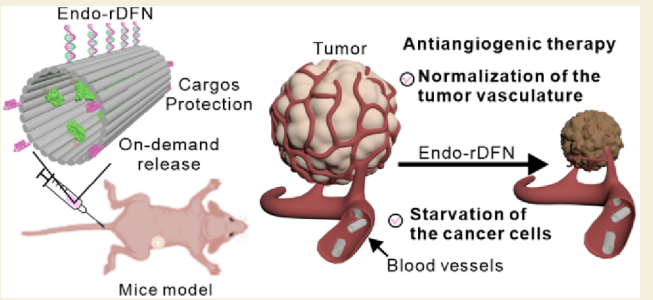

KEYWORDS: *DNA nanotechnique, DNA framework, antiangiogenic therapy, endostar, multiorgan injury*

INTRODUCTION

Antiangiogenic therapy, which targets tumor blood vessels-related molecules for inhibiting the growth of tumor blood vessels and the development of tumors has emerged as one of the most attractive cancer treatment strategies.[1,2] With the burgeoning development of antiangiogenic therapy, a multitude of antiangiogenic drugs have been applied to cancer treatment in clinic or in basic studies.[3,4] These antiangiogenic drugs have remarkably prolonged the survival time of cancer patients, and their combination with the first-line chemotherapeutic drugs even contributed to the definition of some certain cancers toward a chronic disease owing to the synergistic effects.[5−7] However, antiangiogenic drugs often cause multiorgan injury, such as hepatotoxicity and cardiotoxicity due to their poor tumor-targeting performance and nonspecific biodistribution, which finally makes the cancer patients suffer tremendously.[8−12] In this regard, developing a robust platform, capable of facilitating the tumor targeting of antiangiogenic drugs and simultaneously reducing their cumulation in normal tissues, is highly desirable and a precondition for circumventing multiorgan injury.

DNA origami is a self-assembly technology to fold a kilobase single-stranded scaffold into prescribed shapes via the base-pairing interactions with hundreds of short staple strands.[13,14] Based on this self-assembly technology, customized DNA origami structures with adjustable size and dimension can be acquired, and they can serve as nanovehicles for drug delivery or other biological applications such as biologic imaging, biosensing, biocomputation, and biostorage.[15−18] In contrast to other nanovehicles, DNA origami features good biological compatibility, negligible immunogenicity, ignorable toxicity, and high safety as its degradation products (deoxyribonucleotides) are essential elements of the human body.[18,19] More importantly, DNA origami has high programmability, making itself easy to be modified with targeting and release units, which endows the loaded drugs with enhanced tumor targeting ability and controlled release function.[20−22] Owing to the aforementioned distinct advantages, DNA origami-based nanosystem has been utilized for the controlled delivery of coagulation enzymes to induce localized tumor thrombosis.[23] However, to the best of our

Received: October 28, 2023
Revised: February 28, 2024
Accepted: March 15, 2024
Published: March 29, 2024

knowledge, the application of the DNA origami-based self-assembly technique for the controlled delivery of the antiangiogenic agents and the reduction of multiorgan injury remains unexplored.

In this study, we tailor-made a reconfigurable DNA framework nanotube (rDFN) through DNA origami-based self-assembly technique for the targeted delivery of endostar (Endo), a China Food and Drug Administration-approved antiangiogenic drug,[24] to tumor sites and the minimum expose to normal tissues. Two functional elements driven by AS1411, a specific DNA aptamer for tumor-overexpressed nucleolin,[23] were simultaneously introduced into rDFN and played an indispensable role (Scheme 1). On the one hand, the incorporation of AS1411 strands at both termini of rDFN enhanced the tumor targeting and accumulation of Endo through the specific binding interaction between AS1411 and nucleolin. On the other hand, rDFN was secured by a series of fasteners composed of AS1411 strand and its partially complementary DNA strand. The controlled opening of these fasteners in response to tumor-overexpressed nucleolin triggered the transition of Endo-rDFN from a closed, curled-up conformation to an open, stretched-out conformation. This conformational change enabled the localized release of Endo, thereby reducing its exposure to normal tissues and creating a favorable condition for minimizing antiangiogenic therapy-induced multiorgan injury. Moreover, the antitumor effect of Endo in combination with the first-line chemotherapeutic drugs (vincristine and cisplatin) was also investigated, which exhibited a striking shrinkage of tumor size and a prolonged survival span, implying a synergistic therapeutic efficacy in the treatment of nonsmall-cell lung cancer. This study provides a potential avenue for preventing antiangiogenic drugs or other anticarcinogens from causing multiorgan injury in cancer treatment.

Scheme 1. Mechanistic Study of the Endo-rDFN-Assisted Antiangiogenic Therapy[a]

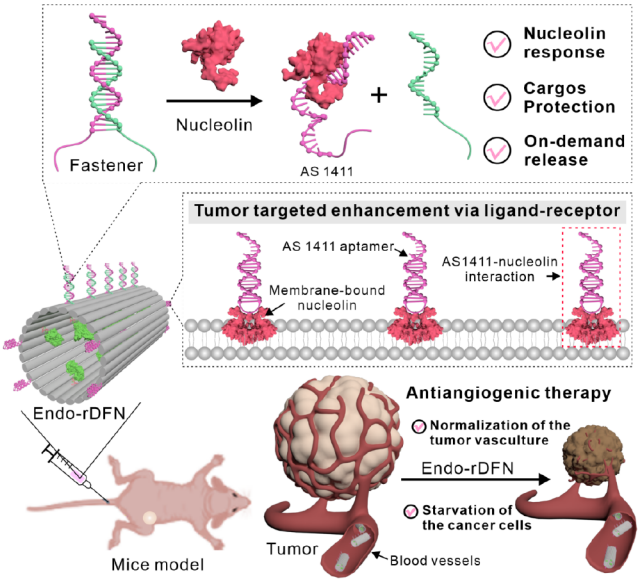

[a]On the one hand, AS1411 strands as the targeting domain added at both ends of rDFN effectively promoted the accumulation of Endo-rDFN at tumor sites. On the other hand, fasteners as the controlled-release domain were employed to fasten Endo-rDFN, which achieved reconfigurable transformation of Endo-rDFN from closed state to open state and the selective exposure of Endo to tumor tissues in response to tumor-overexpressed nucleolin, thus providing a favorable condition for reducing antiangiogenic therapy-evoked multiorgan injury.

RESULTS AND DISCUSSION

Design and Characterization of Endo-rDFN

Before synthesis of the reconfigurable DNA framework nanotube (rDFN), a capture strand-anchored DNA framework nanosheet (Capture-DFS) was first developed by the folding of the M13 DNA scaffold strand with a predesigned staple and capture DNA strands (Figures 1A and S1 and Table S1). Meanwhile, endostar (Endo) was modified with biotin and then conjugated to the biotin-DNA through streptavidin (SA) to form DNA-Endo (Figure S2). Subsequently, DNA-Endo was hybridized with Capture-DFS and loaded onto the surface of DFS (Endo-DFS). To avoid exposing cargo Endo to normal tissues excessively and enhance its tumor enrichment efficiency, 8 pairs of AS1411-associated DNA aptamer strands were mixed with Endo-DFS. After the mixtures were annealed, the rectangular Endo-DFS could be curled up and secured using 8 pairs of the AS1411-associated aptamers, resulting in the tubular Endo-rDFN. The AS1411 aptamer possesses two distinct functional domains: it serves as both the fastener and the targeted ligand of Endo-rDFN (Figure S3). The successfully fabricated Endo-rDFN was verified by the agarose gel electrophoresis (Figure 1B) and fluorescence colocalization imaging results (Figure 1C).

The first domain in Endo-rDFN is a nucleolin-responsive switch (composed of AS1411 and its partially complementary DNA strand). To assess whether nucleolin could induce the unwinding of the fasteners and the opening of Endo-rDFN, a fluorescent strand exchange experiment was conducted by labeling AS1411 with a quencher (3′-BHQ3) and the complementary strand with 5′-Cy5. In the normal condition (absence of nucleolin), the Cy5 fluorescence was initially quenched by the BHQ3 due to their spatial proximity, indicating that the switch was fastened, and Endo-rDFN was under the closed state. However, once the quencher and Cy5 were departed, leading to the recovery of Cy5 fluorescence, which reflected that the switch in Endo-rDFN could be opened and the loaded Endo could be thus exposed (Figure 2A−C). This reconfigurable transformation process of Endo-rDFN from the closed state to open state was further confirmed by atomic force microscopy (AFM) and negatively stained TEM imaging (Figures 2D and S4). The average hydrodynamic diameter of Endo-rDFN was about 118.7 nm, which was smaller than that of DFS (129.7 nm) (Figure S5). The width of the DFS (59.4 ± 4.43 nm) is twice the width of Endo-rDFN (32.4 ± 5.58 nm). The length/width ratio of DFS was about 1.5, and the length/width ratio of Endo-rDFN was about 2.7 (Figure S6). Endo-rDFN showed good stability in an aqueous environment (Figure S7). Scratch healing experiments displayed that Endo-rDFN retained the activity of Endo on inhibiting the migration of endothelial cells (Figure 2E,F). It was previously reported that Endo had the ability to inhibit tumor proliferation.[12] By scratch healing experiments, it was verified that Endo-rDFN also retained the antitumor proliferation ability (Figure S8).

https://doi.org/10.1021/jacsau.3c00661
JACS Au 2024, 4, 1345−1355

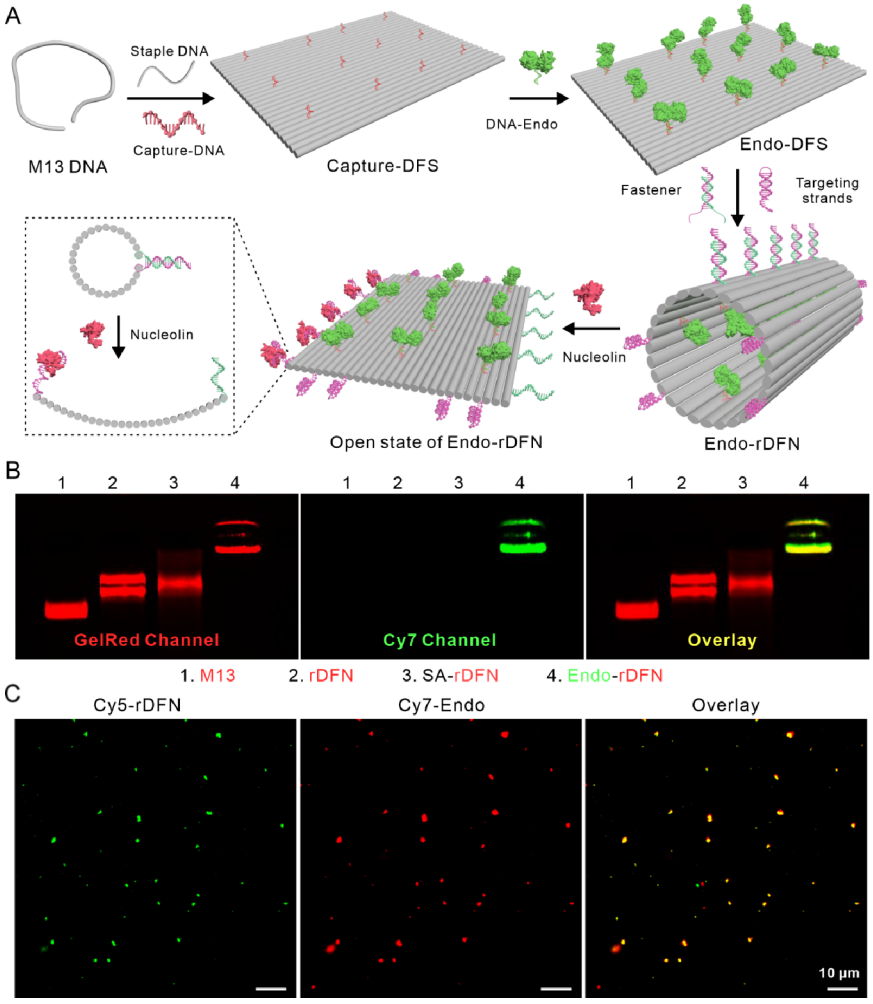

Figure 1. Design and characterization of Endo-rDFN. (A) The schematic illustration showcasing the construction of an Endo-loaded rDFN (Endo-rDFN, closed state) and its reconfiguration into an open state of Endo-rDFN in response to nucleolin binding. (B) The agarose gel electrophoresis of Endo-rDFN. Lane 1: M13 DNA, lane 2: rDFN, lane 3: SA-rDFN, and lane 4: Endo-rDFN. (C) The fluorescence colocalization imaging of Endo-rDFN. The rDFN was labeled with Cy5, and Endo was modified with Cy7.

Biodistribution of Endo-rDFN

The second domain in Endo-rDFN is the tumor-specific targeting domain, which utilizes a specific DNA aptamer AS1411 for recognizing and binding to tumor-overexpressed nucleolin (Figure 3A). Western blot (WB) results indicated that A549 cells (tumor cells) exhibited higher nucleolin expression compared to 16HBE cells (normal cells), as depicted in Figure S9. Characterization to assess the expression level of nucleolin receptors on representative and confocal microscopy images demonstrated the wonderful targeting ability of Endo-rDFN to nucleolin-positive cells (Figure 3A). We have demonstrated the superior targeting ability of Endo-rDFN to tumor cells; we next investigated whether the protective loading could reduce the nonspecific biodistribution of Endo to normal tissues by constructing A549 tumor-bearing mouse models and performing fluorescence imaging. As indicated in Figure 3B, negligible fluorescence signal was observed in Alexa647, Endo, and nontargeted Endo-rDFN groups. In contrast, quantitative analysis (Figure 3C) revealed that Endo-rDFN can accumulate in the tumor 3 times more than that in other groups (***$p < 0.001$). Additionally, the accumulation of Endo-rDFN in the tumor reached a maximum at 12 h after injection (Figure S10). Subsequently, the mice were dissected at 24 and 48 h, and the heart, liver, spleen, lung, kidney, and tumor tissues were collected, and the ex vivo fluorescence imaging was conducted, from which we found the anatomic tumor had the highest fluorescence signal, compared with other organs (heart, liver, spleen, lung, and kidney), at 24 h post the injection of Endo-rDFN (Figure 3D). In addition, ex vivo fluorescence imaging also indicated that Endo-rDFN could accumulate in the tumor for more than 48 h (Figure S11). Collectively, by selectively targeting nucleolin, Endo-rDFN can maximize the delivery of Endo directly to the cancerous site, thus minimizing the potential side effects on healthy tissues.

Long-Term Safety Investigation

Increasing evidence has demonstrated that Endostar (Endo) often causes severe multiorgan injury, particularly cardiac trauma.[25−27] Since Endo-rDFN could reduce the biodistribution and direct exposure of Endo to normal tissues, we investigated whether Endo-rDFN could mitigate Endo-induced multiorgan injury. To evaluate the long-term safety of Endo-rDFN, we conducted a series of experiments, including cardiac function assessment, histopathological analysis, and hematological and biochemical assays. Mice received either Endo alone or Endo-rDFN, and their health status was monitored

https://doi.org/10.1021/jacsau.3c00661
JACS Au 2024, 4, 1345−1355

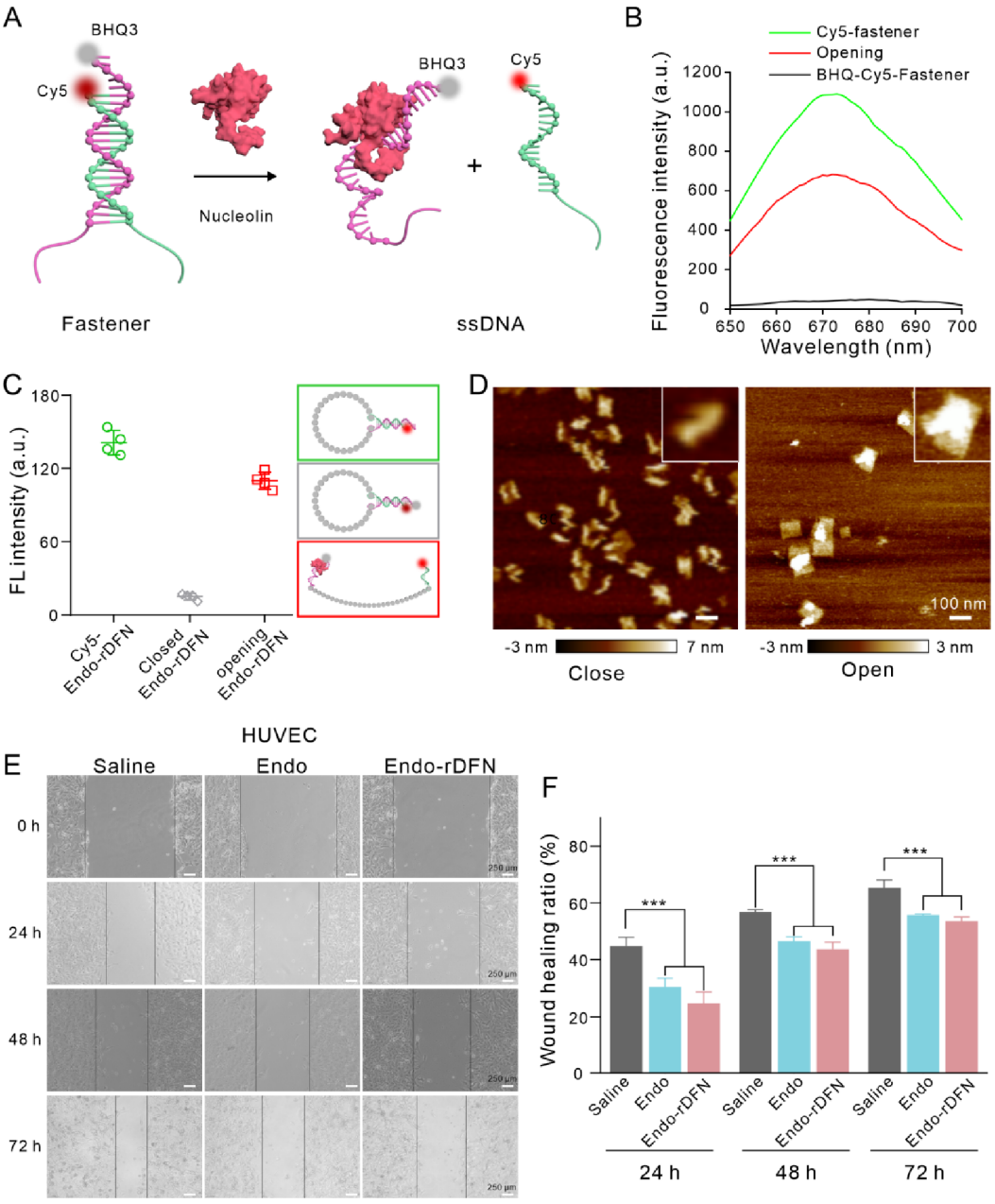

Figure 2. Nucleolin-responsive opening of Endo-rDFN. (A) The schematic illustration showing the opening of fastener when it binds to nucleolin. (B, C) The fluorescence recovery analysis of fastener (B) and Endo-rDFN (C) in response to nucleolin (AS1411 and the complementary DNA modified with BHQ3 and Cy5, respectively). (D) The representative AFM images of Endo-rDFN in closed (left) and open (right) states. (E) Scratch healing experiments of HUVECs after indicated treatments (scale bars = 250 μm). (F) The quantitative analysis of (E). ***$p < 0.001$.

regularly. Cardiac function was assessed using a mouse cardiac ultrasound system. The results revealed that, compared to the control group, mice treated with Endo alone exhibited significant declines in cardiac output, ejection fraction, fractional shortening, stroke volume, and heart rate throughout the study period. In contrast, mice treated with Endo-rDFN exhibited no significant changes in these parameters over time (Figures 4A,B and S12). Histopathological analysis of major organs (heart, liver, spleen, lung, and kidney) was performed at the end of the study period. The results demonstrated that mice treated with Endo alone exhibited evident pathological changes in several organs such as myocardial damage and renal tubular injury. Conversely, mice treated with Endo-rDFN had no detectable pathological alterations in any of the organs examined (Figures 4C and S13). Hematological and biochemical assays were conducted to assess the potential adverse effects of Endo-rDFN. The results showed that mice treated with Endo alone exhibited significant variations in multiple hematological and biochemical parameters, including increased levels of liver enzymes and creatinine as well as decreased red blood cell count, hemoglobin level, and platelet count. In contrast, mice treated with Endo-rDFN had no apparent fluctuations in hematology or biochemical indexes throughout the study period (Figures 4D and S14). Collectively, the long-term safety evaluation demonstrated that Endo alone induced significant multiorgan toxicity, while Endo-rDFN was well tolerated and did not elicit any apparent adverse effects in mice. These findings suggest that Endo-

https://doi.org/10.1021/jacsau.3c00661
JACS Au 2024, 4, 1345−1355

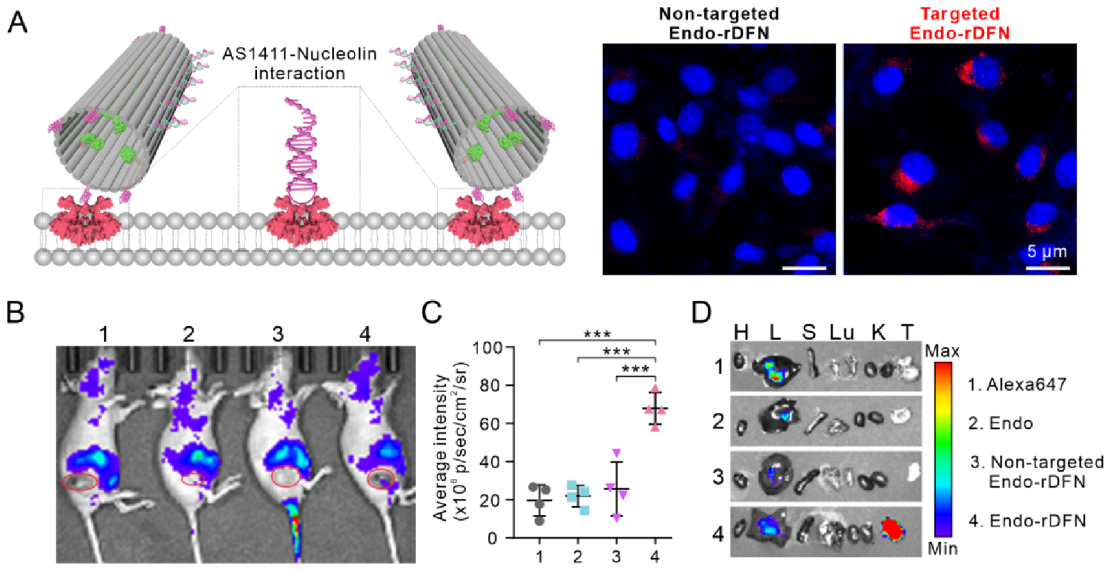

Figure 3. Biodistribution of Endo-rDFN. (A) The targeting schematic diagram (left) and targeting ability of Endo-rDFN to nucleolin-positive HUVECs. (B) The IVIS images of A549 tumor-bearing mice in different groups. (C) The quantitative analysis of (A). ***$p < 0.001$. (D) The IVIS images of the ex vivo organs 24 h post the injection of indicated samples.

rDFN is a safe and effective drug delivery system for Endo. We propose that this efficient drug-targeting delivery system will have significant translational implications for clinical treatment.

In Vivo Antitumor Efficacy

Having proved that the protective loading of Endo with rDFN could reduce the potential side effects to normal tissues, we next wonder whether Endo-rDFN could amplify the antiangiogenic therapy outcome and the combination of Endo-rDFN with vincristine (Vrb) and cisplatin (Ddp), two of first-line chemotherapeutic drugs for nonsmall-cell lung cancer,[28−30] whether could exert better antitumor efficacy. The tumor-bearing A549 nude mice were randomly divided into five groups: saline, Endo-, Endo-rDFN, Vrb + Ddp-Endo, and Vrb + Ddp-Endo-rDFN (Figure 5A). Among them, Endo and Endo-rDFN were administered by tail vein injection, and Endo was injected once a day 10 times while Endo-rDFN was injected every 2 days for a total of 5 times owing to its better tumor targeting and accumulation effect. Vrb and Ddp were administered by intraperitoneal injection, where Vrb was injected twice every 7 days, while Ddp was injected 3 times, at 1−3 days (Figure 6A). As shown in Figure 5B−D, tumor growth in mice treated with Endo-rDFN was significantly slower than that in saline and Endo treatment groups, suggesting the enhanced antiangiogenic therapy output rendered by rDFN. Furthermore, the combination of Endo-rDFN with Vrb and Ddp exhibited a synergistic antitumor effect with the survival rate improving to 83.3%, 83.3%, 66.7%, and 23.3% compared with saline, Endo, Endo-rDFN, and Vrb + Ddp-Endo groups, respectively (Figure 5E). In addition to the superb antitumor outcome, no significant decline in body weight was observed in Figure 5F, suggesting the absence of any acute complications. Additionally, the antitumor efficacy of additional controls, including Endo + Vrb, Endo + Ddp, Endo-rDFN + Vrb, and Endo-rDFN + Ddp, was also evaluated via TUNEL staining (Figure S15). Endo-rDFN demonstrated superior antitumor efficacy compared to Endo alone, and similar results were observed when combined with Vrb, Ddp, or Vrb + Ddp. Notably, the Endo-rDFN + Vrb + Ddp combination exhibited the most potent antitumor effect. These findings provide further evidence supporting the enhanced antitumor efficacy of Endo-rDFN, particularly in combination with chemotherapeutic drugs.

Antitumor Mechanism

To better depict the antitumor activity, a series of pathological assays were conducted. The immunohistochemical staining result of Ki67 (Figure 6A), a marker of active proliferation, showed a reduced growth rate of tumor cells following Vrb + Ddp-Endo-rDFN treatment, which is indicative of its exceptional antitumor activity. In immunohistochemistry, CD31 is a primary indicator used to demonstrate the presence of endothelial cell tissues and evaluate tumor angiogenesis. Based on Figure 6B, it is evident that Endo-rDFN treatment significantly inhibits tumor angiogenesis, as demonstrated by the decreased expression of CD31. This finding highlights the enhanced antiangiogenic therapy effect conferred by rDFN on Endo. As a result, Endo-rDFN not only led to the normalization of tumor vasculature and the starvation of cancer cells but also sensitized the chemotherapeutic efficacy (Figure 6C).

CONCLUSIONS

In summary, we prepared a reconfigurable DNA framework nanotube (rDFN) based on a self-assembly technique to serve as a nanovehicle for the encasement of endostar (Endo). Due to the introduction of AS1411, a specific DNA aptamer for tumor-overexpressed nucleolin, at both ends of rDFN, the encased Endo could be efficiently delivered to tumor sites. Meanwhile, the additional engagement of AS1411 strand as well as its partially complementary DNA strand can fasten the rDFN, which avoids the exposure of Endo to normal tissues and the off-target toxicity. The fasteners were only opened in response to tumor-overexpressed nucleolin, thus greatly reducing Endo-invoked multiorgan injury. Not only that, in combination with chemotherapy drugs, a synergistic antitumor effect was witnessed. Collectively, our DNA origami-based self-assembly technique sheds a light onto the protection against multiorgan injury caused by Endo or other anticarcinogens in cancer treatment.

https://doi.org/10.1021/jacsau.3c00661
JACS Au 2024, 4, 1345−1355

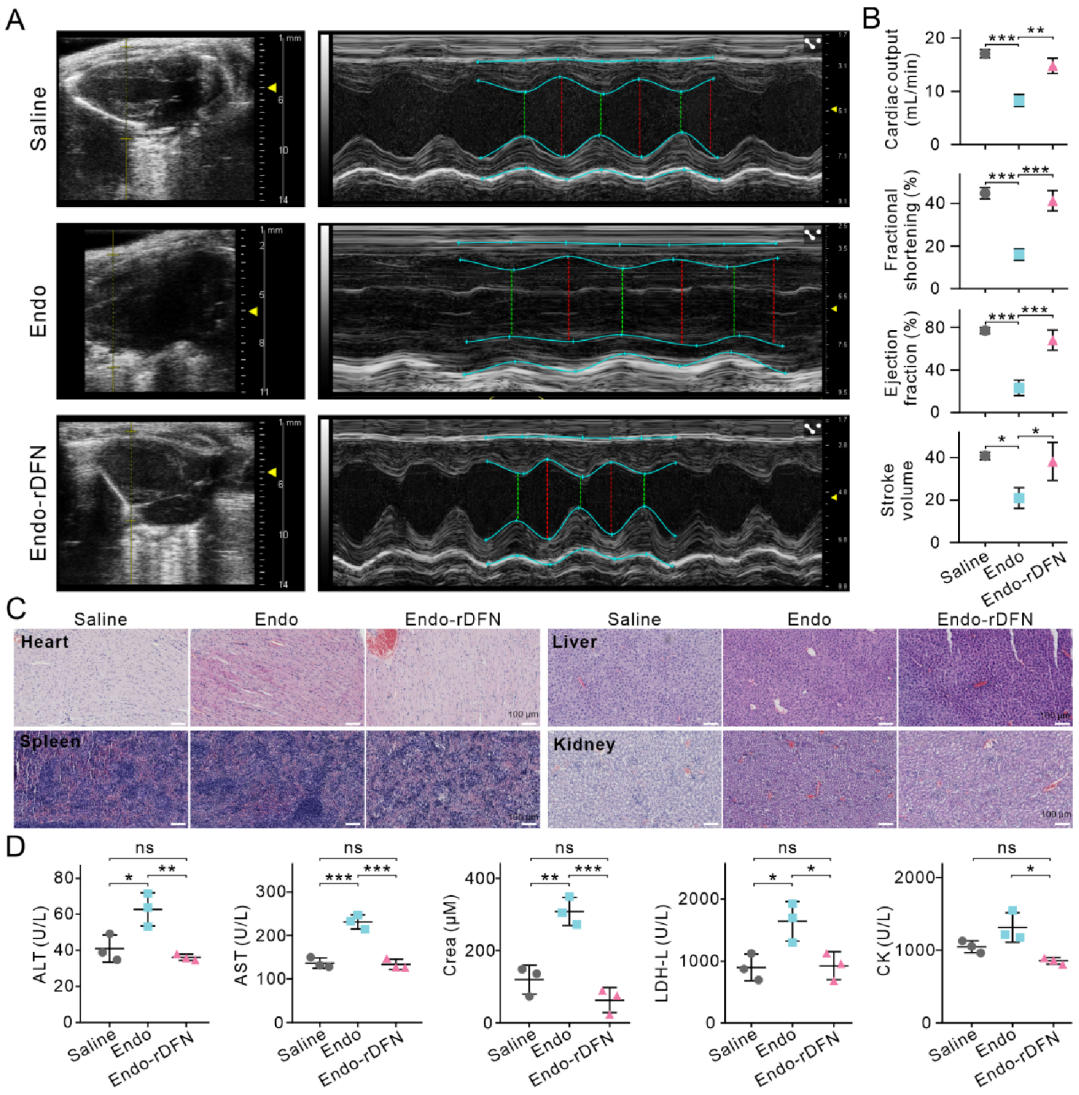

Figure 4. Long-term safety investigation. (A) Cardiac function evaluation by using mouse cardiac ultrasound system. (B) Cardiac output, ejection fraction, fractional shortening, and stroke volume monitoring. (C) H&E staining of the major organs (scale bar = 100 μm). (D) Hematology and biochemical assays testing. *p < 0.05, **p < 0.01, ***p < 0.001, ns: nonsignificant.

EXPERIMENTAL SECTION

Materials

All DNA oligonucleotide strands (staples, capture strands, fastener, and targeting strands) with lengths ranging from 20 to 60 bases were purchased from the BBI Life Sciences Corporation. These strands were dissolved in ultrapure water with a resistivity of 18 MΩ cm. The final concentration of the oligonucleotide strands was 100 μM. M13mp18 single-stranded DNA scaffold (M13 ssDNA) was purchased from Shanghai Liufan Biotechnology Co., Ltd. (catalog number: bayou p-107) and used without further purification. Endostar (Endo) was supplied by Shandong Xiansheng Pharmaceutical Co., Ltd. (Shandong, China). N-Hydroxysuccinimide (NHS, 98.0%) and streptavidin (SA) were purchased from GlpBio. All other chemicals or materials were purchased from Sigma-Aldrich and used as received, unless stated otherwise.

Preparation of Capture-DFS

The Capture-DFS was developed by the folding of the M13 DNA scaffold strand with predesigned staple and capture DNA strands. Briefly, 10 nM M13 mp18 DNA was mixed with 50-fold molar excess staple strands and 100-fold molar excess capture DNA in 1 × TAE-Mg^{2+} buffer (40 mM Tris, 20 mM acetic acid, 2 mM EDTA, and 12.5 mM magnesium acetate, pH = 8.0). The mixture was annealed from 95 to 4 °C. After that, a PEG buffer (15% PEG8000, 5 mM Tris, 1 mM EDTA, and 505 mM NaCl) was added to the mixture in a 1:1 volume ratio and then centrifuged at 10,000g for 15 min. After removing the supernatant, the sediment was resuspended in a 1 × TAE-Mg^{2+} buffer and subjected to shaking at 40 °C, 400 rpm for 8 h.

Modification of Endo with Biotin

100 μL, 1.5 mg/mL Endo was mixed with a 20-fold excess of NHS-biotin (GlpBio, GC135041) in 1 × PBS (pH = 8.0), and the mixture was shaken at 200 rpm, at room temperature for 2 h. After that, the excess NHS-biotin was removed by Zeba spin desalting columns (7 K MWCO, 0.5 mL).

Modification of Endo with NHS-Cy7

Cy7 which contained an N-hydroxysuccinimide activation group (NHS-Cy7) was mixed with Endo in 1 × PBS (pH = 8) for 2 h with a molar ratio of 100:1. Excess NHS-Cy7 was removed by Zeba spin desalting columns (7 K MWCO, 0.5 mL).

Conjugation of Biotin-Endo to Biotin-DNA

Biotin-DNA, SA (GLPBIO, GP247291), and biotin-Endo were mixed in 1 × PBS at a molar ratio of 3:1:1. The mixture was shaken at 200 rpm, at room temperature for 2 h. After that, the excess biotin-DNA was removed through ultrafiltration (3000g, 10 min) with 30 kDa cutoff filters (Amicon) three times in 1 × PBS (pH = 7.2).

https://doi.org/10.1021/jacsau.3c00661
JACS Au 2024, 4, 1345−1355

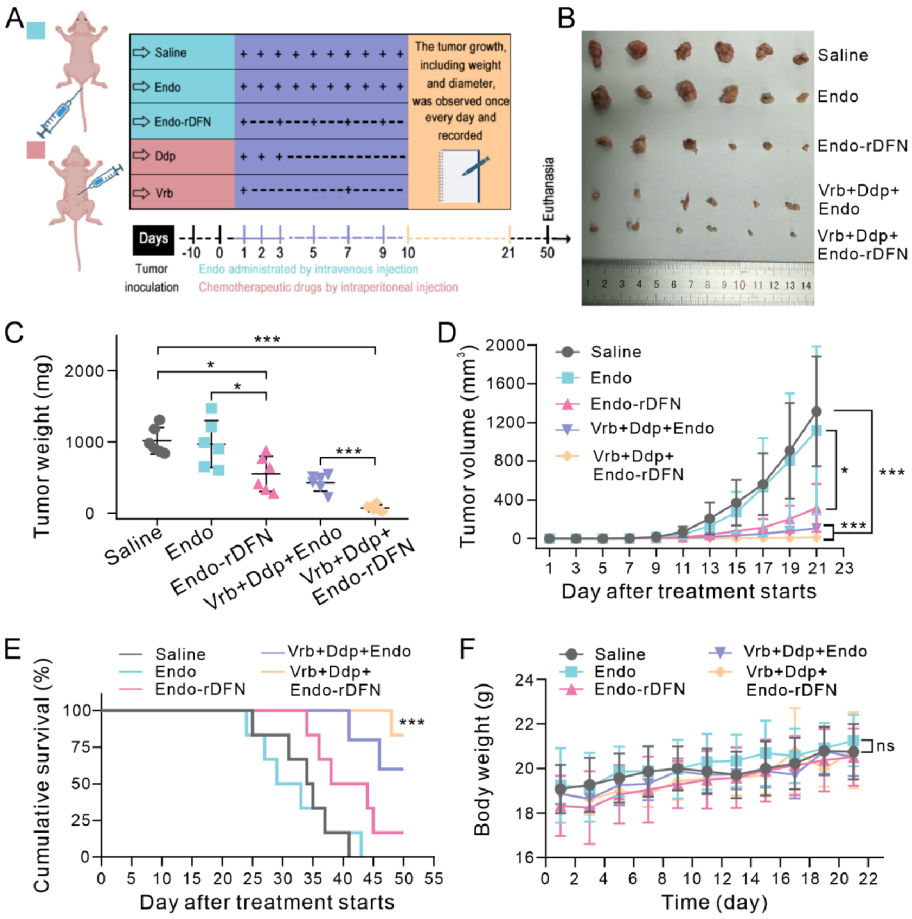

Figure 5. In vivo antitumor efficacy. (A) Schematic diagram of the design for treatment of A549 tumor-bearing mice. (B) Necropsy results of tumors obtained from A549 tumor-bearing mice after indicated treatments. Tumor weight (C) and tumor volume (D) of the treated mice in different groups. Cumulative survival (E) and the body weight (F) of A549 tumor-bearing mice after indicated treatments. *$p < 0.05$, ***$p < 0.001$, ns: nonsignificant.

Endo-Loaded rDFN (Endo-rDFN)

A 5-fold excess DNA-Endo was mixed with Capture-DFS (10 nM) in 1 × TAE-Mg^{2+} buffer. The mixture was annealed from 45 to 25 °C at a rate of 5 min/°C to facilitate the loading of Endo. The mixture was then purified through ultrafiltration (3000*g*, 10 min, 3 times) with 100 kDa to remove excess DNA-Endo conjugates, and Endo-DFS could be obtained. After that, a 30-fold excess of the fastener and a 10-fold excess of targeted strands were added to the Endo-DFS solution (10 nM). To facilitate assembly, the mixture was heated to 45 °C and then cooled to 25 °C at a rate of 5 min/°C. The excess fastener and targeted strands were removed through ultrafiltration (3000*g*, 10 min) with 100 kDa cutoff filters (Amicon) for three times in 1 × TAE-Mg^{2+} buffer.

Characterization

The morphology and conformational transformation of the samples were observed by using atomic force microscopy (AFM; Multimode Nanoscope VIII, Bruker). The hydrodynamic diameter of the samples was monitored by dynamic light scattering (DLS; BI-9000AT, Malvern, UK). The stability and reconfigurable transformation of Endo-rDFN were monitored by using a microplate reader (BioTek, Synergy). Agarose gel electrophoresis experiments were conducted using 1% agarose gel in ice-cold 1 × TAE-Mg^{2+} buffer with a run voltage of 100 V and a run time of 1 h.

Negative-Stain TEM

5 μL of sample containing DNA objects at a concentration of 2−10 nM was pipetted onto a plasma-treated carbon grid. The sample droplets were incubated on the grids for 3 min and then blotted away using filter paper. A 5 μL droplet of 2% aqueous uranyl formate (UFO) solution containing 25 mM sodium hydroxide was pipetted onto the grid and immediately blotted away. Subsequently, a 20 μL UFO droplet was pipetted onto the grid, incubated for 30 s, and blotted away. The grids were air-dried for 20 min before imaging on an FEI Tecnai G2 F20 S-TWIN microscope at 200 kV.

Fastener Duplex Opening by Recombinant Nucleolin

A pair of fluorophore-quencher fasteners was chosen to evaluate the response upon binding to recombinant nucleolin. The Fastener-48 strand was modified with Cy5 at the 5′ end, and its complementary strand (Comp-48) was modified with BHQ3 at the 3′ end. The Cy5-Fastener-48 strand and Comp-48-BHQ3 were mixed in 1 × TAE-Mg^{2+} buffer with a final concentration of 20 μM. The mixture was annealed from 95 to 25 °C at a rate of 3 min/°C.

The DNA sequences used are shown below:

Cy5-Fastener-48: 5-Cy5-GGTGGTGGTGGTTGTGGTGG-TGGTGGTCTAAAGTTTTGTCGTGAATTGCG-3;

Comp-48-BHQ3: 5-GTAAAGCTTTTTTTTTTTTACAACC-ACCACCACC-BHQ3-3.

The fluorophore-quencher fastener (2 μM) was mixed with a 20-fold molar excess of recombinant nucleolin (RPC242Hu01, CloudClone Corp.) at 37 °C. Fluorescence intensity measurements were then performed using a microplate reader (BioTek, SYNERGY H1).

Endo-rDFN Opening by Recombinant Nucleolin

Six pairs of fasteners were designed to lock Endo-rDFN. In order to evaluate the reconfiguration of Endo-rDFN, six pairs of fasteners were modified with fluorophore-quencher pairs and served as switchable fluorescent beacons. These fasteners were mixed in 1 × TAE-Mg^{2+}

https://doi.org/10.1021/jacsau.3c00661
JACS Au 2024, 4, 1345−1355

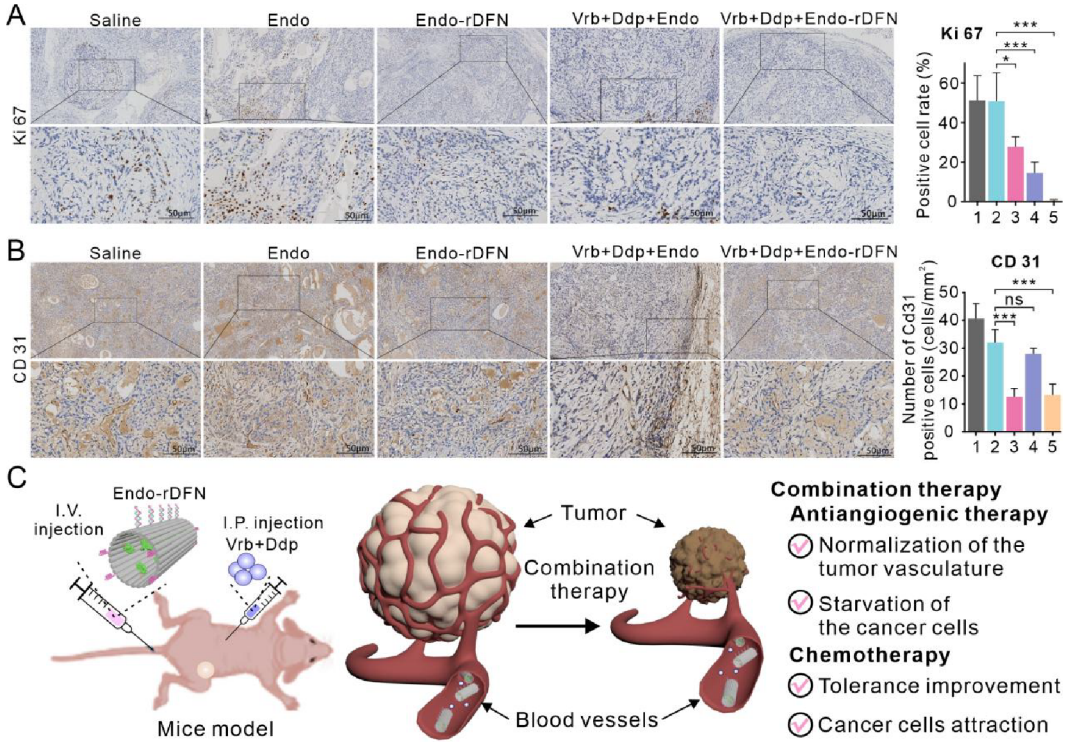

Figure 6. Antitumor mechanism. Representative Ki67 (A) and TUNEL-stained (B) tumor sections of A549 tumor-bearing mice after indicated treatments (scale bar = 50 μm). (C) Schematic diagram showing the combinational therapeutic regimen (I.V. injection of Endo-rDFN for antiangiogenic therapy; I.P. injection Vrb and Ddp for chemotherapy). After the combinational therapy, the tumor angiogenesis and tumor cell proliferation were significantly inhibited. *p < 0.05, ***p < 0.001, ns: nonsignificant.

buffer with the final concentration of 20 μM. The mixture was annealed from 95 to 25 °C at a rate of 3 min/°C. After that, a 30-fold excess of fluorophore-quencher fasteners were added to the Endo-DFS solution (10 nM). To facilitate assembly, the mixture was heated to 45 °C and then cooled to 25 °C at a rate of 5 min/°C. The excess fluorophore-quencher fasteners were removed through ultrafiltration (3000g, 10 min) with 100 kDa cutoff filters (Amicon) three times in 1 × TAE-Mg^{2+} buffer.

The DNA sequences used are shown below:

Cy5-Fastener-48: 5-Cy5-GGTGGTGGTGGTTGTGGTGGTGGTCTAAAGTTTTGTCGTGAATTGCG-3;

Comp-48-BHQ3: 5-GTAAAGCTTTTTTTTTTTTACAACCACCACCACC-BHQ3-3.

Cy5-Fastener-73: 5-Cy5-GGTGGTGGTGGTTGTGGTGGTGGTGGTAGAGCTTGACGGGGAAATCAAAA-3;

Comp-73-BHQ3: 5-TGTAGCATTTTTTTTTTTTTACAACCACCACCACC-BHQ3-3;

Cy5-Fastener-97: 5-Cy5-GGTGGTGGTGGTTGTGGTGGTGGTGGCGAGAAAGGAAGGGAACAAACTAT-3;

Comp-97-BHQ3: 5-TGAGTTTCTTTTTTTTTTTTACAACCACCACCACC-BHQ3−3;

Cy5-Fastener-120: 5-Cy5-GGTGGTGGTGGTTGTGGTGGTGGTGGATAGGAACCCATGTACAAACAGTT-3;

Comp-120-BHQ3: 5-CAAGCCCATTTTTTTTTTTTTACAACCACCACCACC-BHQ3-3;

Cy5-Fastener-144: 5-Cy5-GGTGGTGGTGGTTGTGGTGGTGGTGGCACCACCCTCATTTTCCTATTATT-3;

Comp-144-BHQ3: 5-CCGCCAGCTTTTTTTTTTTTACAACCACCACCACC-BHQ3-3;

Cy5-Fastener-169: 5-Cy5-GGTGGTGGTGGTTGTGGTGGTGGTGGCTACATTTTGACGCTCACCTGAAA-3;

Comp-169-BHQ3: 5-CCCTCAGTTTTTTTTTTTTTACAACCACCACCACC-BHQ3-3.

30 nM Endo-rDFN, labeled with fluorophore-quencher fasteners, was mixed with a 20-fold molar excess of recombinant nucleolin at 37 °C. Fluorescence intensity measurements were then performed using a microplate reader (BioTek, SYNERGY H1).

The Fluorescence Colocalization Imaging of Endo-rDFN

Cy7-labeled Endo was loaded onto Cy5-labeled rDFN to form Cy7-Endo-rDFN-Cy5. The excess Cy7-Endo was removed through ultrafiltration (3000g, 10 min) with 100 kDa cutoff filters (Amicon) for three times in 1 × TAE-Mg^{2+} buffer. 100 μL of the Cy7-Endo-rDFN-Cy5 was dropped onto a glass-bottom dish (D29-10-1.5-N, Cellvis) for 20 min. Co-localization images of Endo and rDFN were then obtained by using fluorescence microscopy (Leica, THUNDER Imager DMI8, German).

Cell Line Culture

Lung adenocarcinoma cell line A549, human bronchial epithelial-like cell line 16HBE, and human umbilical vein endothelial cell line HUVECs were purchased from the American Type Culture Collection (ATCC, USA). Lung adenocarcinoma cell line A549 and human bronchial epithelial-like cell line 16HBE were cultured in RPMI-1640 medium (Bionind, Israel) containing 10% fetal bovine serum (FBS, Procell, China), 100 U/mL penicillin, and 100 U/mL streptomycin. HUVECs were cultured in DMEM supplemented with 10% fetal bovine serum, 100 U/mL penicillin, and 100 U/mL streptomycin. Cells were maintained at 5% CO_2 under 37 °C and routinely tested for mycoplasma contamination.

Scratch Healing Experiment

In a six-well plate, an appropriate amount of cells were inoculated and incubated for 24 h. When the cell density in the field of view reached more than 90% under the microscope, the cells were incubated with 2% low serum for 0, 24, 48, and 72 h using a 200 mL pipet tip crossed vertically with a line at the bottom. Subsequently, the medium was discarded, and the cell migration distance was observed under a bright field microscope.

https://doi.org/10.1021/jacsau.3c00661
JACS Au 2024, 4, 1345−1355

Western Blotting Assay

Cells were collected with 1.5 mL EP tubes, and cytosolic proteins were extracted using a cell membrane extraction kit (Abmart, China #A10008S) mixed with corresponding protease inhibitors and phosphatase inhibitors (Cwbiotech, China) according to the manufacturer's instructions. Protein concentration was determined using a BCA protein concentration assay kit (Beyotime) according to the manufacturer's instructions. Equal amounts of proteins were separated in 10% SDS-PAGE, and then the proteins were transferred to PVDF membranes, closed with 5% skim milk powder for 2 h at room temperature, and then incubated overnight at 4 °C with a 1:1000 dilution of protein primary antibody. The membrane was washed 3 times with TBST, then incubated with conventional secondary antibody for 1 h at room temperature, and washed three more times with TBST. Next, the signal intensity of the membrane was detected using the ECL (enhanced chemiluminescence) Western blotting substrate (Pierce, Rockford, IL) according to the manufacturer's instructions. The following primary antibodies were used: nucleolin (Abmart no. T510696S), β-actin (Abmart no. T40104), and ATPase (Abmart #T55159F).

Cell Targeting of Endo-rDFN

Cells in the logarithmic growth phase were inoculated in six-well plates that were pre-equipped with cell crawlers. The cells were cultured for 24 h until fully attached to the wall. The original medium was discarded, and the cells were washed with PBS. The cells were then cultured for another 24 h in 10% FBS medium. After that, the cells were exposed to Cy5-labeled targeted-Endo-rDFN and non-targeted-Endo-rDFN for 24 h to investigate their targeting properties. Subsequently, the original medium in the well plates was discarded, and the cells were washed with PBS three times, followed by the addition of 4% paraformaldehyde and fixation for 15 min. The fixative was then discarded, and the plates were washed with PBS three times for 5 min each time. Next, the cells were stained with DAPI staining solution for 5 min at 37 °C, followed by discarding the staining solution and washing the plates with PBS three times for 5 min each time. Finally, the stained cells were sealed with an antifluorescence burst sealer and observed under a fluorescence microscope.

Establishment of a Tumor-Bearing Mouse Model

In this experiment, human lung adenocarcinoma A549 cells were used to construct a tumor-bearing mouse model. When the cells grew to an 80% fusion rate and good cell morphology was observed, the cells were digested with trypsin and centrifuged. Subsequently, the supernatant was discarded, and the cells were resuspended with a basal medium. The cell density was adjusted to 5×10^7 cells/mL, and the cell suspension was placed on ice to maintain the viability of the cells. Subsequently, 100 μL (i.e., 5×10^6) of A549 cells was inoculated subcutaneously in the right lower limb of each female BALB/c nude mouse as soon as possible (within 1 h) to establish a female BALB/c nude mouse model of lung adenocarcinoma cancer with A549 cells. Each tumor-bearing nude mouse was labeled with an ear stud and observed every other day for bulging at the injection site. Tumor volume (V) was measured with vernier calipers, $V = LWH \times \pi/6$ (L, W, and H are the length, width, and thickness of the tumor, respectively). When the tumor size and volume averaged about 100 mm^3, the next step of the experiment could be performed. All experiments were approved by the Animal Care and Use Committee of Zhujiang Hospital, Southern Medical University (LAEC-2022-176).

Biodistribution Investigation

Biodistribution investigation was conducted by in vivo and ex vivo fluorescence imaging. For in vivo fluorescence imaging, A549 tumor-bearing mouse models were randomly divided into 4 groups ($n = 4$): Alexa647, Endo, nontargeted Endo-rDFN, and Endo-rDFN (Endo in each group was labeled with Alexa647). Subsequently, the samples were injected through the tail vein (the dose of Alexa647 was 5 nmol for each individual). At 1, 2, 4, 6, 8, 12, 24, and 48 h after the administration, the mice were anesthetized with isoflurane, and the distribution of fluorescence was observed on a Multispectral Imaging System (PerkinElmer, USA). For ex vivo fluorescence imaging, the mice were euthanized at the time point of 24 and 48 h. Then, the tumor, heart, liver, spleen, lung, and kidney were rapidly dissected and separated. Subsequently, fluorescence imaging (emission wavelength 680 nm, excitation wavelength 640 nm) was performed on a Multispectral Imaging System (PerkinElmer, USA).

In Vivo Antitumor Efficacy

When the tumor volume reached about 100 mm^3, the tumor-bearing mice were randomly divided into 5 groups ($n = 6$) and injected intravenously with physiological saline (200 μL in the control group), Endo, Endo-rDFN, Vrp + Ddp + Endo, and Vrp + Ddp + Endo-rDFN via tail vein (the dose of Endo was 6600 μg/time). As note, Endo was injected once a day while Endo-rDFN was injected every other day, for a total of 10 days per mouse. Vrp and Ddp were administered intraperitoneally, with Vrp administered on days 1 and 8 (the dose was uniformly 15 mg/kg) and Ddp administered on days 1−3 (the dose was 6 mg/kg). The length, width, and thickness of tumors were recorded with vernier calipers, and the weight was weighed and recorded with an electronic balance for 21 days after administration. Survival was monitored up to 50 days, during which dead mice were dissected and tumors were collected. On day 50, the mice that were still alive were euthanized and dissected. Subsequently, the tumors were collected, washed with saline, and stored in 4% paraformaldehyde solution and −80 °C refrigerator, respectively, for histological examination and immunohistochemical analysis. Immunohistochemical analysis of the expression of Ki67, tunnel, and CD31 in different groups in tumor tissue sections was carried out, and representational images were obtained.

In Vivo Biosafety Evaluation

The mice were randomly divided into three groups: saline (control group), Endo, and Endo-rDFN ($n = 3$ for each group), and then the samples (the dose of Endo was uniformly 6600 μg/time) were administered by tail vein injection for 14 days. The hearts of mice were examined by small animal ultrasonography on days 7−14. The blood was collected for hematology and biochemical assays. After execution of nude mice, the heart, liver, spleen, lung, and kidney were rapidly dissected and separated and put into 4% paraformaldehyde for histological examination.

Statistical Analysis

IBM SPSS 21.0 statistical software was applied for data analysis. Measures that conformed to a normal distribution were presented as mean ± standard deviation ($\bar{x} \pm s$) for statistical description. Independent t test was used to assess the differences between groups when comparing only two groups, and one-way ANOVA was used when comparing more than two groups, and the LSD method was used to compare two within groups when the variance was the same, and Dunnett's T3 method was used when the variance was not the same. Asterisks are leveraged to depict the significant differences (*$p < 0.05$, **$p < 0.01$, ***$p < 0.001$, ns: nonsignificant).

■ ASSOCIATED CONTENT

Data Availability Statement

The data sets generated during and/or analyzed during the current study are available from the corresponding authors upon reasonable request.

Supporting Information

The Supporting Information is available free of charge at https://pubs.acs.org/doi/10.1021/jacsau.3c00661.

Schematic display of the folding strategy for DFS (Figure S1); conjugation of Endo with DNA (Figure S2); schematic display of the folding strategy for DFN (Figure S3); negatively stained TEM image of the Endo-DFN (Figure S4); hydrodynamic diameter of DFS and Endo-rDFN characterized by dynamic light scattering (Figure S5); sizes of DFS and Endo-rDFN (Figure S6);

https://doi.org/10.1021/jacsau.3c00661
JACS Au 2024, 4, 1345−1355

stability of Endo-rDFN in aqueous solution (Figure S7); scratch healing experiments of A549 cells after different treatments (Figure S8); plasma membrane nucleolin in 16HBE and A549 cells (Figure S9); in vivo fluorescence imaging (Figure S10); IVIS images of the ex vivo organs 48 h post the injection of different samples (Figure S11); monitoring of heartbeat after indicated treatments (Figure S12); H&E staining of the lung (Figure S13); hematology and biochemical assaytesting (Figure S14); TUNEL staining of tumor sections for evaluating cell apoptosis after indicated treatments (Figure S15); and sequence of short single-stranded oligonucleotides used in this study (Table S1) (PDF)

AUTHOR INFORMATION

Corresponding Authors

Linlang Guo − *Department of Pathology, Zhujiang Hospital, Southern Medical University, Guangzhou, Guangdong 510282, China*; Email: linlangg@yahoo.com

Chao Zhang − *Department of Oncology, Zhujiang Hospital, Southern Medical University, Guangzhou, Guangdong 510282, China*; Email: czhangsinap@163.com

Jian He − *Department of Nuclear Medicine, Nanjing Drum Tower Hospital, The Affiliated Hospital of Nanjing University Medical School, Nanjing 210008, China*; orcid.org/0000-0003-4580-1381; Email: hjxueren@126.com

Authors

Wei Li − *Department of Oncology, Zhujiang Hospital, Southern Medical University, Guangzhou, Guangdong 510282, China; Department of Endocrinology and Metabolism, 481 Center for Diabetes and Metabolism Research, West China 482 Hospital, Sichuan University, Chengdu 610041, China*

Zhongliang Wang − *Department of Pathology, Zhujiang Hospital, Southern Medical University, Guangzhou, Guangdong 510282, China*

Qing Su − *Department of Pharmacy, Zhujiang Hospital, Southern Medical University, Guangzhou, Guangdong 510282, China*

Jie Chen − *Department of Radiation Oncology, Cancer Hospital of Shantou University Medical College, Shantou, Guangdong 515000, China*

Qian Wu − *Department of Pathology, Beijing Sixth Hospital, Beijing University, Beijing 100080, China*

Xue Sun − *Department of Pathology, Zhujiang Hospital, Southern Medical University, Guangzhou, Guangdong 510282, China*

Shuhan Zhu − *Department of Pathology, Zhujiang Hospital, Southern Medical University, Guangzhou, Guangdong 510282, China*

Xiaodie Li − *Department of Oncology, Zhujiang Hospital, Southern Medical University, Guangzhou, Guangdong 510282, China*

Hao Wei − *Department of Urology, Affiliated Hospital of Qingdao University, Qingdao University, Qingdao, Shandong 266000, China*

Jialin Zeng − *Department of Oncology, Zhujiang Hospital, Southern Medical University, Guangzhou, Guangdong 510282, China*

Complete contact information is available at: https://pubs.acs.org/10.1021/jacsau.3c00661

Author Contributions

◆W.L. and Z.W. contributed equally. W.L. contributed to conceptualization, methodology, software, data curation, writing—original draft. Z.W. contributed to visualization, methodology, data curation, writing—original draft preparation. Q.S. contributed to resources, supervision. Q.W. contributed to methodology, data curation. J.C. contributed to visualization. S.Z.: contributed to software. X.L. contributed to methodology. H.W. contributed to supervision. J.Z. contributed to data curation. L.G. contributed to writing—review and editing. J.H. contributed to writing—review and editing. C.Z.: contributed to writing—review and editing, supervision, funding acquisition, project administration. W.L. and Z.W. contributed equally to this work. All authors have given approval to the final version of the manuscript.

Notes

The authors declare no competing financial interest.

ACKNOWLEDGMENTS

This work was financially supported by the National Natural Science Foundation of China (No. 82373393, No. 22304072), Guangdong Basic and Applied Basic Research Foundation (No. 2022A1515110845, No. 2023A1515011042), and Science and Technology Program of Guangzhou (No. 2023A04J0060).

REFERENCES

(1) Motzer, R. J.; Martini, J. F.; Mu, X. J.; Staehler, M.; George, D. J.; Valota, O.; Lin, X.; Pandha, H. S.; Ching, K. A.; Ravaud, A. Molecular Characterization of Renal Cell Carcinoma Tumors from a phase III Anti-Angiogenic Adjuvant Therapy Trial. *Nat. Commun.* **2022**, *13* (1), 5959.

(2) Msaouel, P.; Goswami, S.; Thall, P. F.; Wang, X.; Yuan, Y.; Jonasch, E.; Gao, J.; Campbell, M. T.; Shah, A. Y.; Corn, P. G.; et al.etal. A phase 1−2 trial of Sitravatinib and Nivolumab in Clear Cell Renal Cell Carcinoma following Progression on Antiangiogenic Therapy. *Sci. Transl. Med.* **2022**, *14* (641), No. eabm6420.

(3) Liang, P.; Ballou, B.; Lv, X.; Si, W.; Bruchez, M. P.; Huang, W.; Dong, X. Monotherapy and Combination Therapy Using Anti-Angiogenic Nanoagents to Fight Cancer. *Adv. Mater.* **2021**, *33* (15), No. e2005155.

(4) Wei, Z.; Liang, P.; Xie, J.; Song, C.; Tang, C.; Wang, Y.; Yin, X.; Cai, Y.; Han, W.; Dong, X. Carrier-Free Nano-Integrated Strategy for Synergetic Cancer Anti-Angiogenic Therapy and Phototherapy. *Chem. Sci.* **2019**, *10* (9), 2778−2784.

(5) Zhang, Y.; Yang, N.; Dong, Z.; Wu, J.; Liao, R.; Zhang, Y.; Zhang, G.; Ren, M.; Wang, F.; Dong, X.; Liang, P. Dual-Targeting Biomimetic Nanomaterials for Photo-/Chemo-/Antiangiogenic Synergistic Therapy. *ACS Appl. Mater. Interfaces* **2023**, *15* (28), 33288−33298.

(6) Lai, X.; Liu, X. L.; Pan, H.; Zhu, M. H.; Long, M.; Yuan, Y.; Zhang, Z.; Dong, X.; Lu, Q.; Sun, P.; Lovell, J. F.; Chen, H. Z.; Fang, C. Light-Triggered Efficient Sequential Drug Delivery of Biomimetic Nanosystem for Multimodal Chemo-, Antiangiogenic, and Anti-MDSC Therapy in Melanoma. *Adv. Mater.* **2022**, *34* (10), No. e2106682.

(7) Virumbrales-Munoz, M.; Ayuso, J. M.; Loken, J. R.; Denecke, K. M.; Rehman, S.; Skala, M. C.; Abel, E. J.; Beebe, D. J. Microphysiological Model of Renal Cell Carcinoma to Inform Anti-Angiogenic Therapy. *Biomaterials* **2022**, *283*, 121454.

(8) Lei, Y.; Duan, J.; Zhang, Q.; Li, Q. Comparation of EGFR-TKI (EGFR tyrosine kinase inhibitors) combination therapy and osimertinib for untreated EGFR-mutated advanced non-small cell

lung cancers: A systematic review and network meta-analysis. *Medicine* **2023**, *102* (30), No. e34483.
(9) Maimaitiming, N.; Ma, X. L.; Wei, Y.; Cao, L. Y.; Gao, Y.; Zhang, L. Efficacy and Safety of Endostar Combined with Chemoradiotherapy versus Chemoradiotherapy alone in Locally Advanced Cervical Cancer: A PRISMA-Compliant Systematic Review and Meta-Analysis. *Medicine* **2022**, *101* (36), No. e30170.
(10) Zhou, J.; Wang, L.; Zhuang, H.; Qin, S.; Xu, X. Safety and Efficacy of Endostar Combined with Platinum-based Chemotherapy in the first-line Treatment of Recurrence and Metastatic Cervical Cancer: A Single-Arm, Prospective Phase II study. *Ann. Oncol.* **2021**, *32*, S754−S754.
(11) Huang, H.; Zhang, C.; Wang, X. L.; Shao, J. S.; Chen, C.; Li, H. M.; Ju, C. M.; He, J.; Gu, H. Y.; Xia, D. L. Overcoming Hypoxia-Restrained Radiotherapy Using an Erythrocyte-Inspired and Glucose-Activatable Platform. *Nano Lett.* **2020**, *20* (6), 4211−4219.
(12) Xiao, L. J.; Yang, S. C.; Hao, J. H.; Yuan, X.; Luo, W.; Jiang, L. P.; Hu, Y.; Fu, Z. P.; Zhang, Y.; Zou, C. Endostar Attenuates Melanoma Tumor Growth via its Interruption of b-FGF Mediated Angiogenesis. *Cancer Lett.* **2015**, *359* (1), 148−154.
(13) Zhang, C.; Yuan, Y. F.; Wu, K. J.; Wang, Y.; Zhu, S. T.; Shi, J. Y.; Wang, L. H.; Li, Q.; Zuo, X. L.; Fan, C. H.; Chang, C.; Li, J. Driving DNA Origami Assembly with a Terahertz Wave. *Nano Lett.* **2022**, *22* (1), 468−475.
(14) Zhang, C.; Jing, X. X.; Guo, L. J.; Cui, C. J.; Hou, X. L.; Zuo, T. T.; Liu, J. B.; Shi, J. Y.; Liu, X. G.; Zuo, X. L.; Li, J.; Chang, C.; Fan, C. H.; Wang, L. H. Remote Photothermal Control of DNA Origami Assembly in Cellular Environments. *Nano Lett.* **2021**, *21* (13), 5834−5841.
(15) Ouyang, X.; Wu, Y.; Guo, L.; Li, L.; Zhou, M.; Li, X.; Liu, T.; Ding, Y.; Bu, H.; Xie, G.; et al.et al. Self-assembly Induced Enhanced Electrochemiluminescence of Copper Nanoclusters Using DNA Nanoribbon Templates. *Angew. Chem., Int. Ed.* **2023**, *62* (21), No. e202300893.
(16) Yin, J.; Xie, M.; Wang, J.; Cui, M.; Zhu, D.; Su, S.; Fan, C.; Chao, J.; Li, Q.; Wang, L. Gold-Nanoparticle-Mediated Assembly of High-Order DNA Nano-Architectures. *Small* **2022**, *18* (22), No. e2200824.
(17) Sun, Y.; Yan, L.; Sun, J.; Xiao, M.; Lai, W.; Song, G.; Li, L.; Fan, C.; Pei, H. Nanoscale Organization of two-Dimensional Multimeric pMHC Reagents with DNA Origami for $CD8^+$ T Cell Detection. *Nat. Commun.* **2022**, *13* (1), 3916.
(18) Sun, Y.; Sun, J.; Xiao, M.; Lai, W.; Li, L.; Fan, C.; Pei, H. DNA Origami-based Artificial Antigen-Presenting Cells for Adoptive T Cell Therapy. *Sci. Adv.* **2022**, *8* (48), No. eadd1106.
(19) Hao, Y.; Li, M.; Zhang, Q.; Shi, J.; Li, J.; Li, Q.; Fan, C.; Wang, F. DNA Origami-Based Single-Molecule CRISPR Machines for Spatially Resolved Searching. *Angew. Chem., Int. Ed.* **2022**, *61* (34), No. e202205460.
(20) Cao, S. T.; Wang, F.; Wang, L. H.; Fan, C. H.; Li, J. DNA Nanotechnology-Empowered Finite State Machines. *Nanoscale Horiz.* **2022**, *7* (6), 578−588.
(21) Zhang, Y. N.; Qu, Z.-B.; Jiang, C.; Liu, Y.; Narayanan, R.; Williams, D.; Zuo, X.; Wang, L.; Yan, H.; Liu, H.; Fan, C. Prescribing Silver Chirality with DNA Origami. *J. Am. Chem. Soc.* **2021**, *143* (23), 8639−8646.
(22) Liu, F.; Li, N.; Shang, Y.; Wang, Y.; Liu, Q.; Ma, Z.; Jiang, Q.; Ding, B. A DNA-Based Plasmonic Nanodevice for Cascade Signal Amplification. *Angew. Chem., Int. Ed.* **2022**, *61* (22), No. e202114706.
(23) Li, S. P.; Jiang, Q.; Liu, S. L.; Zhang, Y. L.; Tian, Y. H.; Song, C.; Wang, J.; Zou, Y. G.; Anderson, G. J.; Han, J. Y.; Chang, Y.; Liu, Y.; Zhang, C.; Chen, L.; Zhou, G. B.; Nie, G. J.; Yan, H.; Ding, B. Q.; Zhao, Y. L. A DNA Nanorobot Functions as a Cancer Therapeutic in response to a Molecular Trigger in vivo. *Nat. Biotechnol.* **2018**, *36* (3), 258−264.
(24) Liu, Y.; Huang, N.; Liao, S.; Rothzerg, E.; Yao, F.; Li, Y.; Wood, D.; Xu, J. Current Research Progress in Targeted Anti-Angiogenesis Therapy for Osteosarcoma. *Cell Proliferation* **2021**, *54* (9), No. e13102.
(25) Zhang, C.; Huang, P. T.; Zhang, Y.; Chen, J.; Shentu, W. H.; Sun, Y.; Yang, Z. J.; Chen, S. Y. Anti-Tumor Efficacy of Ultrasonic Cavitation is Potentiated by Concurrent Delivery of Anti-Angiogenic Drug in Colon Cancer. *Cancer Lett.* **2014**, *347* (1), 105−113.
(26) Qi, X. J.; Zhao, Y. L.; Yang, S.; Sun, Y. M.; Liu, H. L.; Liu, P. Y.; Feng, S. Y.; Tui, H.; Yuan, Z.; Yang, J. K.; Bu, H. Combined Effects of Programmed Cell Death-1 Blockade and Endostar on Brain Metastases of Lung Cancer. *Anti-Cancer Agents Med. Chem.* **2023**, *23* (6), 709−716.
(27) Cunningham, C.; Bolcaen, J.; Bisio, A.; Genis, A.; Strijdom, H.; Vandevoorde, C. Recombinant Endostatin as a Potential Radiosensitizer in the Treatment of Non-Small Cell Lung Cancer. *Pharmaceuticals* **2023**, *16* (2), 219.
(28) Jiang, W. X.; Cai, G. Q.; Hu, P.; Wang, Y. Personalized Medicine of Non-Gene-Specific Chemotherapies for Non-Small Cell Lung Cancer. *Acta Pharm. Sin. B* **2021**, *11* (11), 3406−3416.
(29) Sei, S.; Mussio, J. K.; Yang, Q. E.; Nagashima, K.; Parchment, R. E.; Coffey, M. C.; Shoemaker, R. H.; Tomaszewski, J. E. Synergistic Antitumor Activity of Oncolytic Reovirus and Chemotherapeutic Agents in Non-Small Cell Lung Cancer Cells. *Mol. Cancer* **2009**, *8*, 47.
(30) Gan, P. P.; Pasquier, E.; Kavallaris, M. Class III Beta-Tubulin Mediates Sensitivity to Chemotherapeutic Drugs in Non-Small Cell Lung Cancer. *Cancer Res.* **2007**, *67* (19), 9356−9363.

https://doi.org/10.1021/jacsau.3c00661
JACS Au 2024, 4, 1345−1355